Published in final edited form as:

Biomaterials. 2014 February ; 35(6): 1967–1976. doi:10.1016/j.biomaterials.2013.10.075.

Multimodal Nanoprobes to target cerebrovascular amyloid in Alzheimer's disease brain

Kristen M. Jaruszewski[a,b,d], **Geoffry L. Curran**[b], **Suresh K. Swaminathan**[a], **Jens T. Rosenberg**[e], **Samuel C. Grant**[e,f], **Subramanian Ramakrishnan**[e,f], **Val J. Lowe**[c], **Joseph F. Poduslo**[b], and **Karunya K. Kandimalla**[a,b,*]

[a]Department of Pharmaceutics and Brain Barriers Research Center, College of Pharmacy, University of Minnesota, Minneapolis, MN 55455, USA

[b]Molecular Neurobiology Laboratory, Department of Neurology, Neuroscience and Biochemistry/Molecular Biology, Mayo Clinic College of Medicine, Rochester, MN 55905, USA

[c]Nuclear Medicine, Department of Radiology, Mayo Clinic, Rochester, MN 55905, USA

[d]Department of Pharmaceutics, College of Pharmacy and Pharmaceutical Sciences, Florida A&M University, Tallahassee, FL 32307, USA

[e]The Florida State University and National High Magnetic Field Laboratory, Tallassee, FL 32310, USA

[f]Department of Chemical and Biomedical Engineering, College of Engineering, Florida A&M University-Florida State University, Tallahassee, FL 32310, USA

Abstract

Cerebral amyloid angiopathy (CAA) results from the accumulation of Aβ proteins primarily within the media and adventitia of small arteries and capillaries of the cortex and leptomeninges. CAA affects a majority of Alzheimer's disease (AD) patients and is associated with a rapid decline in cognitive reserve. Unfortunately, there is no pre-mortem diagnosis available for CAA. Furthermore, treatment options are few and relatively ineffective. To combat this issue, we have designed nanovehicles (nanoparticles-IgG4.1) capable of targeting cerebrovascular amyloid (CVA) and serving as early diagnostic and therapeutic agents. These nanovehicles were loaded with Gadolinium (Gd) based (Magnevist®) magnetic resonance imaging contrast agents or single photon emission computed tomography (SPECT) agents, such as ^{125}I. In addition, the nanovehicles carry either anti-inflammatory and anti-amyloidogenic agents such as curcumin or immunosuppressants such as dexamethasone, which were previously shown to reduce cerebrovascular inflammation. Owing to the anti-amyloid antibody (IgG4.1) grafted on the surface, the nanovehicles are capable of specifically targeting CVA deposits. The nanovehicles effectively marginate from the blood flow to the vascular wall as determined by using quartz crystal microbalance with dissipation monitoring (QCM-D) technology. They demonstrate excellent distribution to the brain vasculature and target CVA, thus providing MRI and SPECT contrast specific to the CVA in the brain. In addition, they also display the potential to carry therapeutic agents to reduce cerebrovascular inflammation associated with CAA, which is believed to trigger hemorrhage in CAA patients.

---

[*]Corresponding author. Department of Pharmaceutics, College of Pharmacy, University of Minnesota, 308 Harvard St. SE, 9-149A Weaver-Densford Hall, Minneapolis, MN 55455, USA. Tel.: +1 612 624 3715; fax: +1 612 626 2125. kkandima@umn.edu, kaarunya@gmail.com (K.K. Kandimalla).

Keywords

Cerebrovascular amyloid (CVA); Brain targeting; Alzheimer's disease (AD); Nanovehicles; Magnetic resonance imaging (MRI); Single photon emission computed; tomography (SPECT)

1. Introduction

Cerebral amyloid angiopathy (CAA) currently affects a majority of Alzheimer's disease (AD) patients and one third of the aging population over 60 years of age. The AD patients with CAA display more pronounced build-up of amyloid beta (Aβ) 40 and 42 proteins within cerebral arteries and arterioles than those without CAA. The accumulation of these toxic Aβ proteins leads to cerebrovascular inflammation, vascular dysfunction, microhemorrhages in the early stages, but in advanced stages lobar hemorrhages and massive strokes are predominant [1].

Currently, there is neither a treatment nor a definitive pre-mortem diagnosis available for CAA. Theoretically, magnetic resonance imaging (MRI) has sufficient spatial resolution and contrast to visualize cerebrovascular amyloid (CVA) and aid in CAA diagnosis. However, the detection of deposits less than 35 μm, which is critical for the early diagnosis of CAA, will require contrast enhancement [2]. Development of monocrystalline iron oxide nanoparticles (MIONs) as MRI contrast agents to detect CVA has been previously attempted [3]. However, this approach addresses CAA diagnosis but not the treatment. In addition, MIONs cannot be tuned for detection via other functional modalities such as positron emission tomography (PET) and SPECT imaging. The objective of the current project is to develop a nanovehicle capable of: a) specifically targeting CVA; b) serve as PET or MRI contrast agent for the early detection of CAA; and c) function as a drug delivery vehicle carrying effective doses of anti-oxidants or immunosuppressants to the cerebral vasculature ridden with amyloid deposits.

2. Materials and methods

Monoclonal antibody raised against human fibrillar Aβ42, IgG4.1, was developed at the Mayo Clinic [4], whereas DutchAβ40 was synthesized by the Mayo Clinic Proteomics Core Facility (Rochester, MN). SuperSignal West Dura extended duration chemiluminescent substrate and Bicinchoninic acid (BCA) protein assay kit were acquired from Thermo Scientific (Rockford, IL). The Mini-Protean® TGX™ 4–15% gel was obtained from Bio-Rad (Hercules, CA). AlexaFluor 647 (AF647) labeling kit was attained from Invitrogen (Carlsbad, CA). Fetal bovine serum and Dulbecco's modified Eagle's medium (DMEM) were acquired from Mediatech Inc. (Manassas, VA). Quartz crystals coated with gold (100 nm) were purchased from Biolin Scientific® (Sweden). All other chemicals were purchased from Sigma Chemical Co (St. Louis, MO).

2.1. Animals

B6/SJL mice were obtained from Jackson Laboratory (Bar Harbour, ME). Swedish Tg2576 transgenic mice were purchased from Taconic (Germantown, NY). All procedures were approved by the Mayo Clinic Institutional Animal Care and Use Committee and were performed in strict accordance with National Institutes of Health Guide for the Care and Use of Laboratory animals. Animals were housed in a non-barrier facility under controlled light and temperature.

2.2. Cell culture

Human brain microvascular endothelial cells (hCMEC/D3) were obtained under license from INSREM France and cultured as described previously [5]. The hCMEC/D3 cells were seeded on the Transwells® (12 mm, Costar, Cambridge, MA) pre-coated with 0.1% type 1 rat-tail collagen. The Transwells® were maintained for 7 days at 5% CO_2 and 37 °C until the monolayer displayed transendothelial electrical resistance (TEER) values >175 Ω.

2.3. Nanoparticle preparation

The polymeric nanocore without any surface modification is referred to as nanoparticle in this manuscript.

2.3.1. Hydroxypropyl-beta-cyclodextran and drug (HPβCD [drug]) complexation—An aliquot of 50 mg HPβCD was added to 10 ml distilled water and continuously stirred overnight at room temperature. The next day, either 1.25 mg/ml of curcumin in acetone or 6.25 mg/ml dexamethasone in ethanol was added, allowed to equilibrate overnight, and the ethanol or acetone was allowed to evaporate for an additional 4 h [6].

2.3.2. Conjugation of gadolinium-diethylene triamine pentaacetic acid (Gd-DTPA) to chitosan—An aliquot of 95 mg/ml Gd-DTPA (Magnevist®, Bayer Schering Pharma AG, Germany), was conjugated to 0.5% medium MW chitosan (MW = 190–300 kDa) using the carbodiimide reaction at pH 4.5 for 6 h [7–9]. Free GD-DTPA was removed by dialyzing the conjugated preparation against distilled water using a Spectrapor 7 dialysis membrane with an MW cut-off (MWCO) of 50 kDa.

2.3.3. Formation of nanoparticles—Curcumin or dexamethasone loaded nanoparticles were prepared using the ionic gelation technique at pH 5.0. The HPβCD complex was slowly added to GD-DTPA-chitosan dispersion in a 2:9 ratio. The chitosan then was crosslinked with 0.05% tripolyphosphate (TPP) to form the nanoparticles.

2.4. Preparation of nanovehicles (nanoparticles-IgG4.1)

The IgG4.1 nanoparticle is referred to as nanovehicle in this manuscript. The IgG4.1 (600, 1200 or 2400 μg) was conjugated covalently to 60 mg freshly prepared nanoparticles using the carbodiimide conjugation previously developed by our laboratory [3]. Nanovehicles were subjected to ultracentrifugation (131,000 × g; 10 min), which served as a 1-step procedure to remove free IgG4.1 and therapeutic agent. The amount of IgG4.1 retained on the nanovehicle surface was characterized using BCA protein assay.

2.4.1. Substantiation of IgG4.1 conjugation to nanovehicles—Western blot analysis was used to confirm successful conjugation of IgG4.1 to nanovehicles as described earlier [10]. In brief, IgG4.1 solution or IgG4.1 conjugated nanovehicles were incubated with Laemmli sample buffer supplemented with 5% v/v 2-mercaptoethanol; heated in a hot water bath (~82 °C) for 5 min and then centrifuged at 10,000 rpm at 4 °C. The supernatant was then resolved using a 4–15% mini-PROTEAN® TGX™ pre-cast gel and blotted onto a 0.2 μm pore size nitrocel-lulose membrane. The blot was then blocked with 5% non-fat milk in phosphate buffered saline containing 0.05% Tween-20 (PBST), incubated with anti-mouse IgGhorseradish peroxidase antibody for 1 h, washed with PBST and analyzed using SuperSignal West Dura chemiluminescent detection reagent.

2.4.2. Radioiodination—The chloramine-T reaction was used to radiolabel nanovehicles with ^{125}I [PerkinElmer Life and Analytical Sciences, Boston, MA] [11]. Unbound ^{125}I was removed through overnight dialysis of the ^{125}I-nanovehicle against PBS (pH 7.4). The purity of the radiolabeled nanovehicle was determined using the trichloroacetic acid (TCA) precipitation method and confirmed using paper chromatography as outlined previously [12].

2.5. Nanovehicle characterization

The nanovehicle morphology was characterized using atomic force microscope (AFM) equipped with MultiMode Scanning Probe (Veeco Metrology Inc., Plainview, NY). Nanoparticles and nanovehicles were also characterized in terms of particle size (hydrodynamic diameter) and zeta potential using a BI-200SM dynamic laser light scattering system (Brookhaven Instruments, Holtsville, NY) and a Zeta Plus machine (Brookhaven Instruments, Holtsville, NY), respectively.

The amount of Gd-DTPA retained on the nanovehicle surface was quantified by measuring the differences in absorbance of nanovehicles with and without Gd-DTPA at 660 nm with 0.2 M Arsenazo III [13]. The amount of encapsulated curcumin in the nanovehicle formulation was quantified by measuring the fluorescence intensity after ultracentrifugation. To evaluate the curcumin released from the nanovehicles, 625 μg/ml of freshly prepared nanovehicles were placed in a dialysis bag (MWCO 50 kDa) and immersed in a PBS trough at 25 °C. The trough contents were stirred continuously at 200 rpm, sampled at pre-determined time points (1, 2, 4, 8, 16, 21, 25, 36, 48, 62, 72 and 90 h) and the corresponding fluorescent signals were evaluated (Ex/Em: 488/535 nm).

The ability of nanovehicle formulations to recognize and bind to DutchAβ40 was evaluated using an enzyme linked immunosorbent assay (ELISA) method previously developed by our lab. A high protein binding 96-well plate was coated overnight with DutchAβ40, blocked using bovine serum albumin (BSA), and incubated with 7.5 mg nanovehicles at 37 °C for 3 h. The secondary anti-mouse IgG-alkaline phosphatase was used to estimate the amount of IgG4.1 bound to DutchAβ40 [4].

2.6. Nanovehicle characterization using in vitro techniques

Quartz crystal microbalance with dissipation monitoring technology (QCM-D) was used to evaluate the impact of systemic dilution on the propensity of various nanovehicles to marginate towards the BBB endothelium. In addition, the ability of nanovehicles to target CVA was tested by determining the extent of nanovehicle accumulation with the DutchAβ40 treated Madin Darby canine kidney (MDCK) cell monolayer grown on the gold crystal sensors. The polarized MDCK cell monolayers are widely used as *in vitro* BBB models and were chosen for this experiment owing to their durability and compatibility with sensors. The sensors, which are outfitted with gold electrodes were cleaned according to the manufacturers recommended protocol (Q-Sense®, Västra Frölunda, Sweden). The MDCK cells were seeded on the sensor surface at a density of 5000 cells/sensor and were incubated under 5% CO_2 and 37 °C for 5 days. The culture medium, which consisted of 90% DMEM, 10% FBS and 1× penicillin–streptomycin, was changed every 12 h. Before the experiment, the monolayer was incubated with 0.1% BSA in Hank's Buffered Salt Solution (HBSS) and 15 mM HEPES to block non-specific binding. The cell-sensors were placed in the QCM-D chamber (Q-Sense Flow Module QFM 401) maintained at 37 °C, and HBSS-HEPES was passed through the chamber at a flow rate of 0.1 ml/min. Once the equilibration was established and baseline stabilized, either HBSS (control) or 12.5 μg DutchAβ40 (treatment)was introduced over the course of 5 min, followed by 400 μl HBSS-HEPES to remove unbound DutchAβ40 at 100 μl/min. A 10.6 mg/ml aliquot of nanovehicle suspension was introduced at 100 μl/min for 5 min and changes in the sensor frequency were monitored. To evaluate the effect of systemic dilution of the nanoparticles as well as nanovehicles, various concentrations of nanoparticles or nanovehicles were floated across the naked sensor surface at the same flow rate and temperature settings. The changes in frequency were monitored and the mass absorbed to the crystal was calculated as follows:

$$\Delta m = -\frac{\Delta FC}{n} \quad (1)$$

where Δm is the change in mass, ΔF is the change in frequency, C (mass sensitivity constant) is equal to 17.7 ng•cm^{-2}•Hz^{-1} and n (overtone number) is equal to 5.

2.6.1. The uptake of nanovehicles by human BBB in vitro model—An amyloid treated brain endothelial model was prepared by pre-incubating the hCMEC/D3 monolayer (see section 2.2) with 12.5 μg DutchAβ40 protein for 20 min [14]. The protein was removed, and an aliquot of 30 μg/ml AlexaFluor 647 (AF647)-nanovehicles, in which AF647 is conjugated to IgG4.1 on the nanovehicle, was added and incubated for 1 h at 5% CO_2 and 37 °C with minimal shaking. The nanovehicles were removed, cells were harvested, washed with PBS and fixed using 4% para-formaldehyde. The amount of intracellular fluorescent signal was quantified using flow cytometry.

2.6.2. Elucidating the mechanism of nanovehicle uptake by human BBB model in vitro—The human brain endothelial cell model was pre-treated with HBSS (control), 10 μg/ml nystatin (caveolae mediated endocytosis inhibitor) or 5 μg/ml chlorpromazine (clathrin mediated endocytosis inhibitor) for 30 min and then incubated with a 30 μg/ml aliquot of AF647-nanovehicles for 1 h at 5% CO_2 and 37 °C with minimal shaking. The treatment was removed, the monolayers were washed and fixed using 4% paraformaldehyde. The Transwells® were stained with DAPI, mounted, and imaged with an Axiovert 100M microscope equipped with Zeiss LSM 510 laser confocal microscope (DAPI, Ex/Em: 350/470 nm and AF647, Ex/Em: 652/668). To maintain consistency, all images were acquired using the same instrument settings.

2.7. In vivo characterization—To evaluate the brain distribution of nanovehicles, WT mice (20–25 g) were anesthetized (1.5% isoflurane, 4 l/min O_2) and their femoral arteries and veins were catheterized. The mice were pre-injected with DutchAβ40 protein (500 μg; treatment) or normal saline (100 μl; control) via the femoral vein and after 15 min 100 μCi of ^{125}I-nanovehicles were administered to each mouse in control and treatment groups. At pre-determined time points (0.25, 1, 5, 15 and 30 min), 20 μl blood was collected from the femoral artery, the plasma was recovered from the sample, and immediately assayed for radioactivity using a two-channel gamma counter (Cobra II; Amersham Biosciences Inc., Piscataway, NJ). Then the ^{125}I-nanovehicles were removed from the cerebral blood flow using transcardial perfusion with PBS. The brains were excised from the skull, sectioned into six different brain regions, weighed, and assayed for radioactivity.

The plasma kinetic data thus obtained was analyzed using non-compartmental pharmacokinetic analysis (WinNonlin® Professional, version 5.2, Mountain view, CA). The area under the plasma kinetic curve was determined using log-trapezoidal rule:

$$\underset{1-n}{AUC} = \sum \left\{\frac{C_1+C_2}{2}\right\} \times (t_2 - t_1) + \left\{\frac{C_2+C_3}{2}\right\} \times (t_3 - t_2) + \dots \quad (2)$$

where AUC is the area under the curve. The selected time points are t_1, t_2 and t_3 whereas C_1, C_2 and C_3 are the corresponding plasma concentrations. The plasma clearance (CL), volume of distribution at steady state (Vdss) and other pharmaco-kinetic parameters were derived from the plasma data using WinNonlin®.

2.8. Ability of nanovehicles to target cerebrovascular amyloid

Nanovehicle targeting to cerebrovascular vessels was determined by administering 45 mg AF647-nanovehicles via external carotid to 2-year-old APP transgenic or age-matched WT mice. After 25 min, transcardial perfusion with 2 ml/kg Evan's Blue (shown by the blue fluorescence) in PBS followed by 4% paraformaldehyde was performed. Blood vessels including arterioles were isolated using (1.25, 1.5 and 1.75 M) sucrose gradient centrifugation [3]. The 1.5 M isolated fraction was mounted using cytospin, stained with Thioflavin S (marker for CVA deposits) and subsequently imaged using an Axiovert 100M microscope with settings for fluorescein isothiocyanate (Ex/Em: 488/535 nm), Evan's Blue (Ex/Em: 550/610 nm) and AF647 [Ex/Em: 652/668 nm] [3].

2.9. Magnetic resonance imaging (MRI)

All MR images were acquired using a 21.1 T vertical magnet with a bore diameter of 105 mm at the National High Magnetic Field Laboratory (NHMFL) [15–18]. Images and relaxation measurements were acquired with a Bruker Avance III spectrometer equipped with ParaVision 5.1 (Bruker Biospin, Billerica, MA) and a 64-mm inner diameter high performance gradient (Resonance Research Inc, Billerica, MA).

MRI relaxometry measurements were carried out on phantoms containing the Gd-DTPA conjugated nanovehicles. Phantoms were prepared by diluting the nanovehicles in distilled water to obtain a concentration range of 0.72–23 mM Gd. The solutions were injected into micro-capillary tubes and sealed with silicone gel (Dow Corning, Midland, MI). The tubes were imaged in sets of 7 using a 10-mm birdcage coil, tuned to a proton (^{1}H) resonance frequency of 900 MHz. Measurements were performed to quantify R_1 and R_2 relaxation rates for each dilution using a single slice 2D spin-echo (SE) sequence with 9 incrementing repetition times (TR = 25–15,000 ms) and 16 incrementing echo times (TE = 8–124 ms) for each respective relaxation mechanism. Sequences were acquired axially with an in-plane matrix of 128 × 128, 1.0 mm slice thickness, and 2 averages. The images were analyzed using Regions of Interest (ROIs) drawn to cover each individual micro-capillary as well as a noise ROI to perform baseline corrections. The ROI signal intensities were fitted by non-linear regression using the Levenberg–Marquardt algorithm in SigmaPlot 7.101 (SPSS Inc, Chicago, IL); for R_2 measurements, a single exponential decay function with baseline adjustment was employed while a single exponential growth function was applied for R_1.

For *ex vivo* MR imaging, a 200 µl aliquot containing 17 mg of nanovehicles was injected, via the femoral vein, to 2-year-old APP transgenic (Tg2576) or age-matched WT mice (25–30 g). Three hours following the injection, transcardial perfusion was performed with PBS followed by 4% paraformaldehyde. The brains were excised and stored in 4% paraformaldehyde at 4 °C until imaged. One day before MR imaging, the excised brains were washed in PBS then placed individually in conical tubes containing Fluorinert (3M, St. Paul, MN), a perfluorinated liquid with no ^{1}H MRI signal [19, 20]. The brains were imaged in unison using a 33-mm RF birdcage coil resonating at 900 MHz. A 3D gradient recalled echo sequence (GRE)was used to generate high resolution T_2*-weighted images. The matrix was set to achieve a 50-µm isotropic resolution with echo (TE) and repetition (TR) times were set to 10 and 150 ms, respectively. The data set was processed with a Gaussian filter using AMIRA 5.3.3 (Visage Imaging, CA). This software also was used to visualize the brain structures of interest and to compare each brain.

2.10. SPECT imaging

A 500 µCi dose of ^{125}I-nanovehicles was administered to 2-year-old Tg2576 or age-matched WT mice. Cerebral and peripheral organ uptake of ^{125}I-nanovehicle was determined by 15 s/scan dynamic planar imaging, over a 40–60 min time range, using a low energy, high resolution parallel-hole collimator 12.5 cm FOV (X-SPECT, Gamma Medica Ideas Pre-Clinical Imaging, Northridge, CA). Single photon computed tomography (SEPCT) scans with corresponding computed tomography (CT) scans were taken at the completion of the dynamic phase and at set intervals on the X-SPECT Gamma Medica scanner with the following parameters; low energy, high resolution parallel-hole collimator 12.5 cm FOV, 13:36 min acquisition time, 64 projections 10 s per projection, and reported resolution 1–2 um. The CT acquisition was a continuous circular orbit with a 50 um slice thickness, 256 images at 80 kVp with a 0.28 mA current, and reported resolution of 43 um. Dynamic and SPECT/CT images were processed and analyzed using Biomedical Image Quantification and Kinetic Modeling Software version 2.85 (PMOD Technologies, Switzerland). The brain uptake of nanovehicles at various time points was calculated using the following equation:

$$\begin{aligned}&\mathrm{Brainuptake}{=}\mathrm{Amount\ \ of}^{125}\mathrm{I}-\mathrm{NVs\ \ in\ \ the\ \ brain}\\&\quad-({}^{125}\mathrm{I}{-}\mathrm{NV\ \ concentration\ \ in\ \ the\ \ plasma}\times\mathrm{cerebrovascular\ \ volume})\end{aligned}\tag{3}$$

2.11. Statistical analyses

Statistical analysis of ELISA results was conducted using a one-way analysis of variance (ANOVA) followed by Tukey's post-test using GraphPad Prism 5.0 software (GraphPad Software Inc., San Diego, CA). Statistical comparisons of the pharmaco-kinetic parameters were performed using a Student's *t*-test. Biodistribution studies in WT mice, with and without DutchAβ40 treatment, were compared using two-way ANOVA with a Tukey's post-test. All experiments were conducted in triplicate.

3. Results

In the following section, the formulation and characterization of nanovehicles; plasma pharmacokinetics and brain uptake; their ability to target CVA; and their potential as MRI and SPECT contrast agents to detect amyloid deposits in the cerebral vasculature are described.

3.1. Formulation of curcumin- and dexamethasone-nanovehicles

The nanovehicles appeared as spherical particles on AFM micrographs and demonstrated size ranges between 90 and 100 nm (Fig. 1A). These values coincided with the particle sizes measured using dynamic light scattering method. Curcumin-nanoparticles (devoid of IgG4.1) demonstrated a particle size of 97.8 ± 1.8 nm (Fig. 1B) and a zeta potential of 7.0 ± 1.9 mV (Fig. 1C). Similarly, dexamethasone-nanoparticles produced particles of 74.1 ± 2.2 nm in size (Fig. 1B) with a positive zeta potential of 5.6 ± 0.7 mV (Fig. 1C). However, when IgG4.1 was conjugated to the nanovehicle surfaces, the particle size increased to 145 ± 5.4 nm for curcumin-nanovehicles and 157.6 ± 3.4 nm for dexamethasone-nanovehicles (Fig. 1B). The corresponding zeta potential for curcumin-nanovehicles increased to 7.7 ± 0.4 mV, but, the zeta potential for dexamethasone-nanovehicles dropped to 4.5 ± 0.5 mV (Fig 1C). All particle size and zeta potential measurements were conducted at physiological pH.

As determined by the Arsenazo III dye assay, the nanovehicles carried 9.5 ± 0.6 μg/mg of Gd-DTPA on the surface (Fig. 1D). The amount of curcumin and dexamethasone encapsulated was 0.03 ± 0.011 and 1.53 ± 0.02 μg/mg of nanovehicles, respectively (Fig. 1E). Almost 75% of the total amount of curcumin encapsulated in the nanovehicles was released within 90 h (Fig. 1F).

The conjugation of IgG4.1 to nanovehicles was optimal when 20 μg of IgG4.1 per milligram of nanovehicles was used for the carbodiimide conjugation. This resulted in 10.0 ± 0.1 μg and 14.6 ± 0.4 μg of IgG4.1 per milligram of curcumin-nanovehicles and dexamethasone-nanovehicles, respectively (Fig. 2A). Both these nanovehicles have shown 5–7 fold higher binding to DutchAβ40 compared to the nanoparticles without IgG4.1 (Fig. 2B). However, no net change in IgG4.1 conjugated to nanovehicles or the ability of nanovehicles to bind to DutchAβ40 was observed when the IgG4.1 amount was increased to 40 μg per milligram of nanovehicles for the carbodiimide conjugation (Fig. 2A and B). Based on these observations, the optimal concentration of IgG4.1 for nanovehicle conjugation was determined as 20 μg/mg of nanovehicles (Fig. 2B). Western blot analysis verified the successful IgG4.1 conjugation to the nanovehicles (Fig. 2C).

To evaluate the plasma pharmacokinetics and brain uptake of the nanovehicles as well as to elucidate their biodistribution using SPECT imaging, the IgG4.1 on the nanovehicle surface was radio-iodinated using a Chloramine-T reaction. Paper chromatography data presented in Fig. 2D showed that the 1st and the 16th paper fractions contained the most radioactivity. The radioactivity accumulated in the first fraction (origin) was most likely from the nanovehicles, whereas the radioactivity from the later fraction was due to the free ^{125}I, running at the solvent front.

3.2. Migration of nanovehicles towards DutchAb40 treated BBB monolayers in vitro

When the nanovehicles are injected into the systemic circulation, they are subjected to extensive dilution. To investigate the dilution effect on the margination of the nanovehicles from the blood flow to the vessel wall, a QCM-D technology was employed. Nanovehicles passing through a microfluidic channel migrated towards the naked quartz crystal more effectively than the nanoparticles at all dilutions. Although, dilution brought noticeable changes in the kinetics and the extent of margination, nanovehicles still maintained superior margination than the nanoparticles (Fig. 3A). The margination of nanovehicles towards the MDCK cell monolayer grown on the surface of the quartz crystal was 3-fold greater than that towards the bare sensor. When the cell mono-layer was treated with DutchAβ40, the mass of nanovehicles bound to the sensor was determined to be 1190 ng/cm^2, whereas the binding to HBSS treated cell-sensors was 970 ng/cm^2 (Fig. 3B). Furthermore, nanovehicles showed a faster margination towards DutchAβ40 treated cell monolayer than towards the HBSS treated monolayer.

3.3. Uptake of nanovehicles by the human BBB model in vitro

The uptake of AF647-nanovehicles by the polarized hCMEC/D3 monolayers, a well characterized human BBB model, was determined by quantifying the amount of intracellular AF647 fluorescence using flow cytometry. Uptake of AF647-nanovehicles by the hCMEC/D3 cells pre-treated with DutchAβ40 showed a 3-fold increase over the monolayers pre-treated with HBSS (Fig. 4A). However, a modest 2-fold increase in AF647-IgG4.1 antibody (no nanovehicle) uptake was observed in FITC-DutchAβ40 treated hCMEC/D3 cells than in the HBSS treated controls (Fig. 4A).

The z-stack images of hCMEC/D3 cell monolayers treated with chlorpromazine (Fig. 4B. ii), an inhibitor of clathrin mediated endocytosis, demonstrated no appreciable difference in the uptake of AF647-nanovehicles compared to the hCMEC/D3 monolayers treated with HBSS (Fig. 4B. i). However, the hCMEC/D3 monolayers treated with nystatin (Fig. 4B. iii), a caveolae mediated endocytosis inhibitor, showed substantially lower uptake of AF647-nanovehicles compared to those treated with HBSS (Fig. 4B. i).

3.4. Biodistribution of nanovehicles

The distribution of ^{125}I-nanovehicles/mg of brain tissue normalized by the plasma AUC was remarkably higher in DutchAβ40 treated versus saline treated mice (Fig. 5B). The plasma

$AUC_{0–30\ min}$ and volume of distribution at steady state (Vdss) was greater in HBSS pre-injected mice than in DutchAβ40 pre-injected mice. But no appreciable differences in either the elimination rate constant (Kel) or clearance (CL) was observed in DutchAβ40 or HBSS pre-injected mice (Table 1).

3.5. Ability of nanovehicles to target cerebrovascular amyloid

To determine the co-localization of nanovehicles with the CVA, 45 mg of AF647-nanovehicles in 200 μl of normal saline was injected via external carotid artery to 24-month old Alzheimer's disease transgenic mouse (Tg2576) or age-matched WT mice. The AF647-nanovehicles showed enhanced cerebrovascular uptake in Tg2576 mouse and selectively targeted amyloid deposits in the vascular wall (Fig. 6B). However, AF647-nanovehicles were confined to the cerebrovascular endothelium and did not show detectable permeation into the vascular wall in WT mice (Fig. 6A).

3.6. Nanovehicles as imaging agents

Coronal MRI brain scans show contrast enhancement by hypo-intense signal from the region where the nanovehicles are located. The signal loss is likely created by the accumulation of the nanovehicle in the arterioles and its substructure, restricting the water access hence creating a more dominant T_2 contrast rather than T_1 contrast as would otherwise be expected from a Gd-based contrast agent. The contrast enhancement is visualized throughout the cortex and in the radiating arterioles of 2-year-old Tg2576 mice (Fig. 6E and F), where the CVA might be expected, but not in age-matched WT mice (Fig. 6C and D). Live dynamic SPECT imaging was conducted by injecting 500 μCi of ^{125}I-nanovehicles in 2-year-old Tg2576 mice or age-matched WT mice. After subtracting the radioactive counts circulating in the cerebral vasculature from the total brain radioactivity, which was quantified by dynamic SPECT imaging, nearly 2-fold increase in the cerebrovascular accumulation of nanovehicles was observed in Tg2576 mice than in WT mice (Fig. 6G).

4. Discussion

For targeting the CVA, the nanoparticles are expected to cross the BBB and be retained in the basement membrane, where CVA is deposited. To accomplish this goal, the nanovehicles are expected to be smaller than 150 nm to allow for the endothelial cell uptake yet larger than 100 nm to restrict migration through the basement membrane matrix into the brain parenchyma. Therefore, curcumin-and dexamethasone-nanovehicles were formulated to maintain a size range of 140–160 nm (Fig. 1B). Furthermore, the nanovehicles were formulated to maintain a positive zeta potential of 5.0–7.0mV (Fig. 1C) to facilitate their adsorptive endocytosis at the negatively charged BBB endothelium. Our previous studies have shown that this zeta potential range was adequate in promoting transcytosis of the nanovehicles [14]. Gd-DTPA was confirmed to be present on the nanovehicle surface (Fig. 1D).

The amount of curcumin encapsulated in the nanovehicles was around 33 ng curcumin/mg nanovehicle (Fig. 1E). When the nanovehicles were exposed to the aqueous environment, approximately 75% of the entrapped curcumin was released within 90 h (Fig. 1F). This sustained delivery of curcumin to the cerebral vasculature is expected to reduce the inflammation at the affected site. Curcumin possesses anti-oxidant, anti-inflammatory and anti-amyloidogenic properties [21–23]. Curcumin also exists in a dynamic equilibrium of keto and enol tautomers, the latter of which can target Aβ aggregates [24]. Dexamethasone, on the other hand, has been shown to significantly reduce inflammation and the occurrence of microhemorrhages [25]. Of these compounds, curcumin has low bioavailability due to poor solubility and higher enzymatic degradation. To circumvent these issues, we utilized

HPβCD's ability to complex hydrophobic curcumin and the resultant HPβCD [curcumin] was encapsulated in the nanovehicles.

The amount of IgG4.1 conjugated to the nanovehicle surface was quantified using BCA protein assay. A substantial increase in the amount of IgG4.1 conjugated to the nanovehicle surface was observed when the concentration of IgG4.1 used in the carbodiimide reaction was doubled from 10 to 20 µg of IgG4.1 per mg of nanovehicle (Fig 2A). This concentration also resulted in enhanced binding of the nanovehicle to DutchAβ40 (Fig 2B). However, a further increase in IgG4.1 from 20 to 40 µg did not further improve the nanovehicle binding to DutchAβ40 (Fig 2B). Hence, 20 µg IgG4.1/mg nanovehicle was considered as the optimal concentration for the conjugation. The IgG4.1 presence on the nanovehicles was confirmed using western blot. IgG4.1 antibody solution was used as positive control. In both these samples, bands corresponding to antibody heavy and light chains were observed. With NVs, extra slow-migrating bands are also seen which may be due to the partial reduction of the whole IgG4.1 antibody into light and heavy chains. The amount of bound ^{125}I in the ^{125}I-nanovehicle formulation as determined by paper chromatography was nearly 53% (Fig. 2D).

The ability of various nanovehicles to marginate towards the BBB endothelium was evaluated *in vitro* using QCM-D. This technique allows for quantifying the mass of nanoparticles adsorbed to an oscillating quartz crystal at the floor of the microfluidic channel through which the nanovehicle suspension is passed at various flow rates. The quartz crystal oscillation frequency is decreased proportionately to the mass of nanovehicles adsorbed on the crystal surface. Based on the frequency changes, the mass bound to the quartz crystal was calculated using the Sauerbrey equation in Qtools® software (Västra Frölunda, Sweden). The nanoparticles without IgG4.1 showed minimal binding and migration to the bare gold sensor, whereas the nanovehicle with IgG4.1 showed a 3-fold increase in binding to the sensor. More importantly, dilution of the nanovehicle suspension did not affect the extent of nanovehicle binding to the sensor (Fig. 3A); this indicates that the ability of the nanovehicle to marginate to the vessel wall is not substantially disrupted when they are diluted in the systemic circulation. To evaluate the ability of these nanovehicles to marginate towards the BBB endothelium in the cerebral vasculature exposed to Aβ proteins, we seeded MDCK cells on the gold sensors and treated them with DutchAβ40. The nanovehicles showed high binding to both HBSS and DutchAβ40 treated cell surface compared to the bare sensor (Fig. 3B). However, in the presence of DutchAβ40, the nanovehicles showed faster migration rate and increased cellular targeting than in case of HBSS treated cells.

Internalization of AF647-nanovehicles in DutchAβ40 treated hCMEC/D3 endothelial cells was three times as much as in HBSS treated cells (Fig. 4A). On the other hand, AF647-IgG4.1 exhibited only a slight increase in the uptake by DutchAβ40 treated cells compared to HBSS treated control cells (Fig. 4A), which indicates a modest uptake of AF647-IgG4.1 compared to the nanovehicles. It can be inferred from these results that the nanovehicle surface covered by the protonated chitosan chains is most likely responsible for the enhanced uptake of nanovehicles by the hCMEC/D3 endothelial cells. The IgG4.1 conjugated to the nanovehicle surface does not play a major role in enhancing the cellular uptake of nanovehicles, but facilitates their intracellular movement along the path of DutchAβ40 accumulation.

The uptake of AF647-nanovehicles in the nystatin-treated hCMEC/D3 endothelial cell monolayer was significantly lower as compared to the monolayers treated with chlorpromazine or HBSS and nanovehicles (Fig. 4B). On the other hand, no differences in uptake were seen between the monolayers treated with HBSS and nanovehicles or chlorpromazine and nanovehicles (Fig. 4B). This clearly demonstrates that caveolae mediated uptake plays a major role in the uptake of nanovehicles.

The plasma pharmacokinetics and brain uptake of nanovehicles were elucidated in WT mice pre-injected with 500 μg of DutchAβ40. Our previous studies have shown that DutchAβ40, when injected intravenously, accumulates primarily in the cerebral vasculature. Hence, the pre-injection of DutchAβ40 into WT mice provides a more reliable CAA model rather than the Tg2576 mice. Although, these AD transgenic mice were shown to express CVA, the extent of vascular amyloid, which drives the biodistribution of nanovehicles, varies significantly from animal to animal and is more common in older mice (≥2 years old). The plasma pharmacokinetics of nanovehicles in the presence of DutchAβ40 is altered significantly and mimicked the biodistribution of DutchAβ40, which suggests that the nanovehicles are responsive to the presence of amyloid *in vivo*. However, the elimination rate constant (kel) of ^{125}I-nanovehicles did not increase to match that of DutchAβ40, which could have resulted in their rapid elimination from the systemic circulation. Based on the observations that the volume of distribution of nanovehicles increased and AUC decreased in DutchAβ40 treated mice as compared to saline treated mice (Fig. 5A), it can be inferred that the changes in nanovehicle distribution due to the presence of DutchAβ40 is primarily due to better tissue partitioning from the systemic circulation. In agreement with these observations, the distribution of ^{125}I-nanovehicles to all brain regions was 2–3-fold higher in DutchAβ40 treated mice than in the saline treated mice (Fig. 5B).

Isolation of vessels from Tg2576 mice treated with AF647-nanovehicles showed co-localization of the nanovehicles with the CVA, thus confirming the ability of nanovehicles to target amyloid within the cerebral vasculature (Fig. 6B). This selective targeting could facilitate site-directed release of curcumin, dexamethasone, or any other anti-oxidant/immunosuppressant to reduce cerebral hemorrhages resulting from inflammation in CAA.

Relaxation and relaxivity analysis of the phantoms indicated the ability of the nanovehicle to provide contrast for MR imaging (Tables 2 and 3). In WT mice, the nanovehicles did not produce detectable MRI contrast (Fig. 6C and D), whereas, high levels of contrast in the radiating arterioles was seen in Tg2576 mice injected with the nanovehicles (Fig. 6E and F). These results demonstrate the ability of nanovehicles to detect CVA in AD transgenic animals. Similar confirmation also was obtained using SPECT/CT imaging, which showed a 6-fold increase in the accumulation of ^{125}I-nanovehicles in Tg2576 versus WT mice (Fig. 6G). One caveat to the MRI data is that the images were obtained *ex vivo* and at a very high field strength (21.1 T) that is not clinically applicable to achieve high spatial resolution. At this ultra-high field, the dominating hypointense T_2* contrast created by the nanovehicle as it accumulates in arterioles and is internalized intracellularly via caveolae may be altered at lower fields. Although this negative contrast might be considered a false positive (*e.g.* blood residue from the transcardial perfusion can generate similar contrast), the consistent contrast generated in the AD transgenic animals and lack of contrast in control mice coupled with histological data lends credence that the hypointense contrast is highly likely generated from nanovehicles. Hence, work is underway in our laboratory to enhance the contrast of nanovehicles to aid in CVA detection at clinical magnetic field strengths. Notably, the SPECT data was obtained *in vivo* on a pre-clinical imager and can be transitioned, after making relevant changes, to image CAA in patients.

5. Conclusions

We have designed a hydrophilic nanovehicle capable of entrapping hydrophobic drugs and demonstrated its ability to target CVA deposits selectively. These nanovehicles are large enough to be retained in the cerebral vasculature, yet small enough to permeate the BBB endothelium. The nanovehicles can be readily equipped with various imaging agents to facilitate early diagnosis of CAA using a variety of diagnostic tools such as MR, SPECT and fluorescent imaging. These nanovehicles were clearly proven to serve as effective diagnostic agents to detect CVA by MRI and SPECT modalities. In addition, they also displayed the potential to carry therapeutic agents to reduce inflammation associated with CAA, which is believed to trigger hemorrhages in CAA patient.

Acknowledgments

Generous financial assistance provided by the Minnesota Partnership for Biotechnology and Medical Genomics to KKK and JFP. Work at The Florida State University was supported by the National Science Foundation (DMR-0084173), the National High Magnetic Field Laboratory User Collaboration Grant Program awarded to SCG and the American Heart Association Grant-in-Aid (10GRNT3860040).

References

1. Calhoun ME, Burgermeister P, Phinney AL, Stalder M, Tolnay M, Wiederhold KH, et al. Neuronal overexpression of mutant amyloid precursor protein results in prominent deposition of cerebrovascular amyloid. Proc Natl Acad Sci U S A. 1999; 96:14088–14093. [PubMed: 10570203]
2. Jack CR Jr, Marjanska M, Wengenack TM, Reyes DA, Curran GL, Lin J, et al. Magnetic resonance imaging of Alzheimer's pathology in the brains of living transgenic mice: a new tool in Alzheimer's disease research. Neuroscientist. 2007; 13:38–48. [PubMed: 17229974]
3. Poduslo JF, Hultman KL, Curran GL, Preboske GM, Chamberlain R, Marjanska M, et al. Targeting vascular amyloid in arterioles of Alzheimer disease transgenic mice with amyloid beta protein antibody-coated nanoparticles. J Neuropathol Exp Neurol. 2011; 70:653–661. [PubMed: 21760540]
4. Poduslo JF, Ramakrishnan M, Holasek SS, Ramirez-Alvarado M, Kandimalla KK, Gilles EJ, et al. In vivo targeting of antibody fragments to the nervous system for Alzheimer's disease immunotherapy and molecular imaging of amyloid plaques. J Neurochem. 2007; 102:420–433. [PubMed: 17596213]
5. Weksler BB, Subileau EA, Perriere N, Charneau P, Holloway K, Leveque M, et al. Blood-brain barrier-specific properties of a human adult brain endothelial cell line. FASEB J. 2005; 19:1872–1874. [PubMed: 16141364]
6. Jingou J, Shilei H, Weiqi L, Danjun W, Tengfei W, Yi X. Preparation, characterization of hydrophilic and hydrophobic drug in combine loaded chitosan/ cyclodextrin nanoparticles and in vitro release study. Colloids Surf B Bio-interfaces. 2011; 83:103–107.
7. Agyare EK, Curran GL, Ramakrishnan M, Yu CC, Poduslo JF, Kandimalla KK. Development of a smart nano-vehicle to target cerebrovascular amyloid deposits and brain parenchymal plaques observed in Alzheimer's disease and cerebral amyloid angiopathy. Pharm Res. 2008; 25:2674–2684. [PubMed: 18712585]
8. Saha TK, Ichikawa H, Fukumori Y. Gadolinium diethylenetriaminopentaacetic acid-loaded chitosan microspheres for gadolinium neutron-capture therapy. Carbohydr Res. 2006; 341:2835–2841. [PubMed: 17045253]
9. Shikata F, Tokumitsu H, Ichikawa H, Fukumori Y. In vitro cellular accumulation of gadolinium incorporated into chitosan nanoparticles designed for neutron-capture therapy of cancer. Eur J Pharm Biopharm. 2002; 53:57–63. [PubMed: 11777753]
10. Swaminathan SK, Roger E, Toti U, Niu L, Ohlfest JR, Panyam J. CD133-targeted paclitaxel delivery inhibits local tumor recurrence in a mouse model of breast cancer. J Control Release. 2013:280–287. [PubMed: 23871962]
11. Poduslo JF, Curran GL, Wengenack TM, Malester B, Duff K. Permeability of proteins at the blood-brain barrier in the normal adult mouse and double transgenic mouse model of Alzheimer's disease. Neurobiol Dis. 2001; 8:555–567. [PubMed: 11493021]
12. Poduslo JF, Curran GL. Increased permeability of superoxide dismutase at the blood-nerve and blood-brain barriers with retained enzymatic activity after covalent modification with the naturally occurring polyamine, putrescine. J Neurochem. 1996; 67:734–741. [PubMed: 8764602]

13. Rowatt E, Williams RJ. The interaction of cations with the dye arsenazo III. Biochem J. 1989; 259:295–298. [PubMed: 2719647]
14. Jaruszewski KM, Ramakrishnan S, Poduslo JF, Kandimalla KK. Chitosan enhances the stability and targeting of immuno-nanovehicles to cerebro-vascular deposits of Alzheimer's disease amyloid protein. Nanomedicine. 2012; 8:250–260. [PubMed: 21704598]
15. Fu R, Brey WW, Shetty K, Gor'kov P, Saha S, Long JR, et al. Ultra-wide bore 900 MHz high-resolution NMR at the National High Magnetic Field Laboratory. J Magn Reson Imaging. 2005; 177:1–8.
16. Rosenberg JT, Cisneros BT, Matson M, Sachi-Kocher A, Sokoll M, Calixto Bejarano F, et al. Encapsulated gadolinium and dysprosium ions within ultrashort carbon nanotubes for MR microscopy at 11.75 and 21.1 T. Contrast Media Mol Imaging. 2003 (In Press).
17. Rosenberg JT, Sachi-Kocher A, Davidson MW, Grant SC. Intracellular SPIO labeling of microglia: high field considerations and limitations for MR microscopy. Contrast Media Mol Imaging. 2012; 7:121–129. [PubMed: 22434624]
18. Rosenberg JT, Kogot JM, Lovingood DD, Strouse GF, Grant SC. Intracellular bimodal nanoparticles based on quantum dots for high-field MRI at 21.1 T. Magn Reson Med. 2010; 64:871–882. [PubMed: 20575090]
19. Webb AG, Grant SC. Signal-to-noise and magnetic susceptibility trade-offs in solenoidal microcoils for NMR. J Magn Reson B. 1996; 113:83–87. [PubMed: 8888593]
20. Ma Y, Hof PR, Grant SC, Blackband SJ, Bennett R, Slatest L, et al. A three-dimensional digital atlas database of the adult C57BL/6J mouse brain by magnetic resonance microscopy. Neuroscience. 2005; 135:1203–1215. [PubMed: 16165303]
21. Yang F, Lim GP, Begum AN, Ubeda OJ, Simmons MR, Ambegaokar SS, et al. Curcumin inhibits formation of amyloid beta oligomers and fibrils, binds plaques, and reduces amyloid in vivo. J Biol Chem. 2005; 280:5892–5901. [PubMed: 15590663]
22. Goel A, Kunnumakkara AB, Aggarwal BB. Curcumin as "Curecumin": from kitchen to clinic. Biochem Pharmacol. 2008; 75:787–809. [PubMed: 17900536]
23. Lim GP, Chu T, Yang F, Beech W, Frautschy SA, Cole GM. The curry spice curcumin reduces oxidative damage and amyloid pathology in an Alzheimer transgenic mouse. J Neurosci. 2001; 21:8370–8377. [PubMed: 11606625]
24. Yanagisawa D, Amatsubo T, Morikawa S, Taguchi H, Urushitani M, Shirai N, et al. In vivo detection of amyloid beta deposition using (1)(9)F magnetic resonance imaging with a (1)(9)F-containing curcumin derivative in a mouse model of Alzheimer's disease. Neuroscience. 2011; 184:120–127. [PubMed: 21497641]
25. Previti ML, Zhang W, Van Nostrand WE. Dexamethasone diminishes the pro-inflammatory and cytotoxic effects of amyloid beta-protein in cerebrovascular smooth muscle cells. J Neuroinflammation. 2006; 3:18. [PubMed: 16887032]

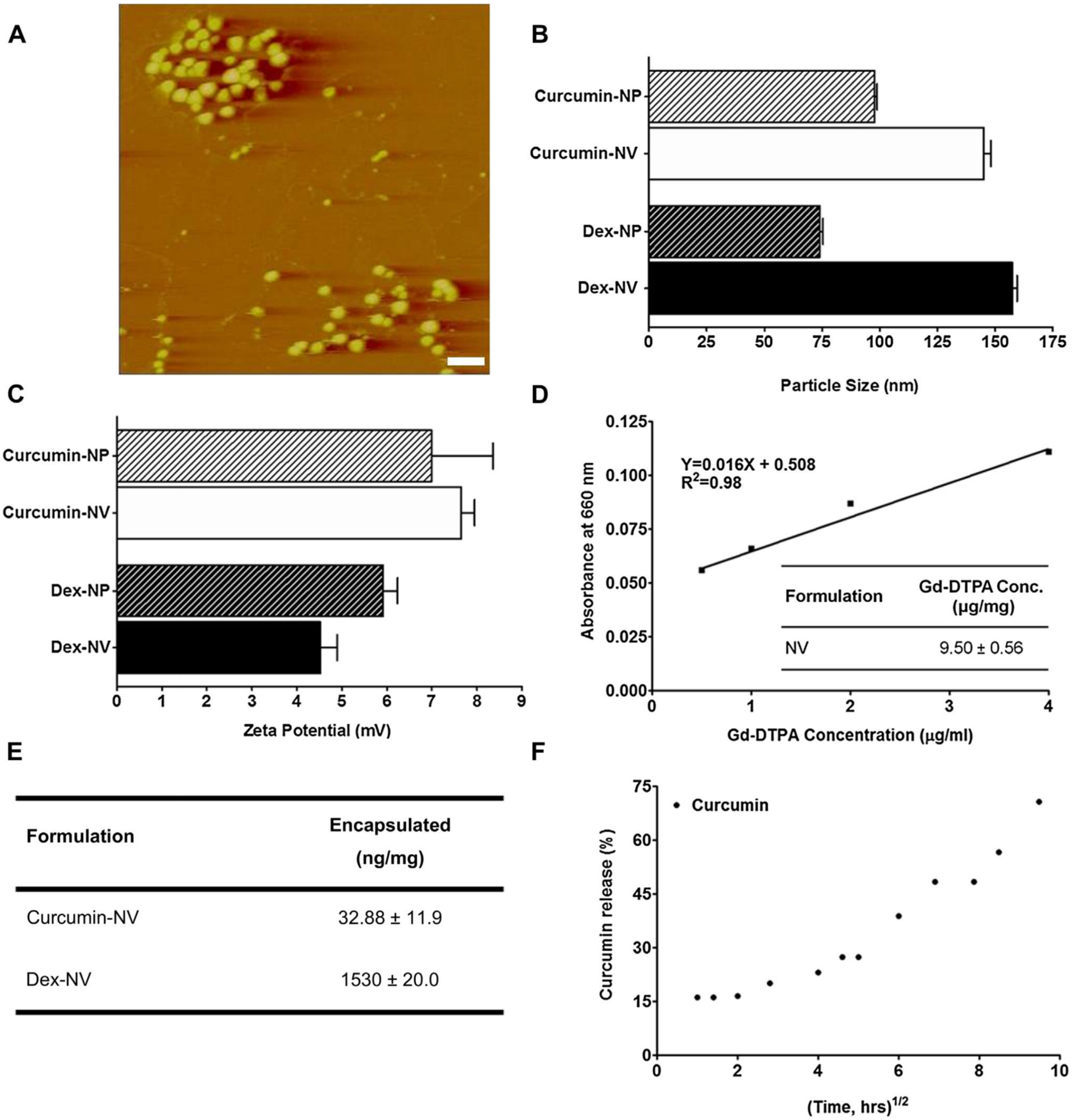

Formulation	Gd-DTPA Conc. (µg/mg)
NV	9.50 ± 0.56

Formulation	Encapsulated (ng/mg)
Curcumin-NV	32.88 ± 11.9
Dex-NV	1530 ± 20.0

Fig. 1.

(A) Atomic force micrograph of nanovehicles (NVs). Scale bar, 250 nm. **(B)** Average particle size of curcumin or dexamethasone (dex) loaded nanoparticles (NP; without IgG4.1) and NVs (with IgG4.1) at pH 7.0 (*n* = 3). **(C)** Effect of pH on the average zeta potential of curcumin or dexamethasone loaded NPs and NVs (*n* = 5). **(D)** Gd-DTPA standard curve with 0.2 mM arsenazo (table insert). The amount of Gd-DTPA present on the surface of Gd-DTPA-NVs as determined by measuring absorbance in the presence of arsenazo II (660 nm). **(E)** The amount of encapsulated curcumin or dexamethasone in the NVs formulation. **(F)** The release of curcumin from the NVs.

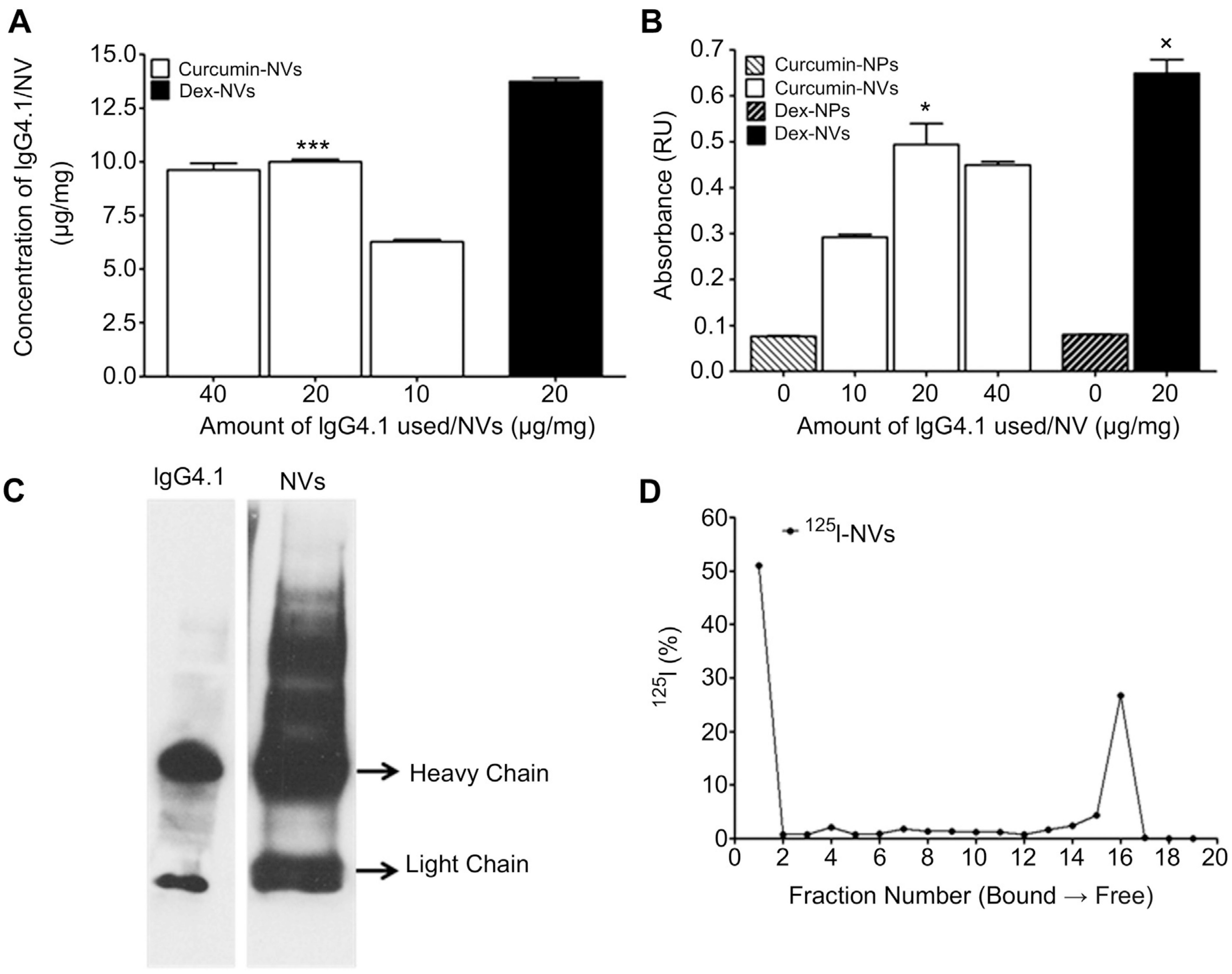

Fig. 2.

(A) The amount of IgG4.1 retained in curcumin or dexamethasone (dex) loaded nanovehicles (NVs; contains IgG4.1). $^{*}p < 0.05$ ($n = 3$); 20 µg of IgG4.1/mg curcumin-NVs vs 10 µg of IgG4.1 g/mg curcumin-NVs. **(B)** Binding of NVs to 10 µg/ml fibrillar DutchAβ40. $^{*}p < 0.005$ ($n = 3$); 14 mg of IgG4.1/mg curcumin-NVs and dexamethasone-NVs vs 7 mg of IgG4.1/mg curcumin-NVs. **(C)** Substantiation of IgG4.1 conjugation to the NVs by Western blot. **(D)** The percentage of free and bound ^{125}I in the ^{125}I-IgG4.1 conjugated nanovehicle formulation as shown by paper chromatography.

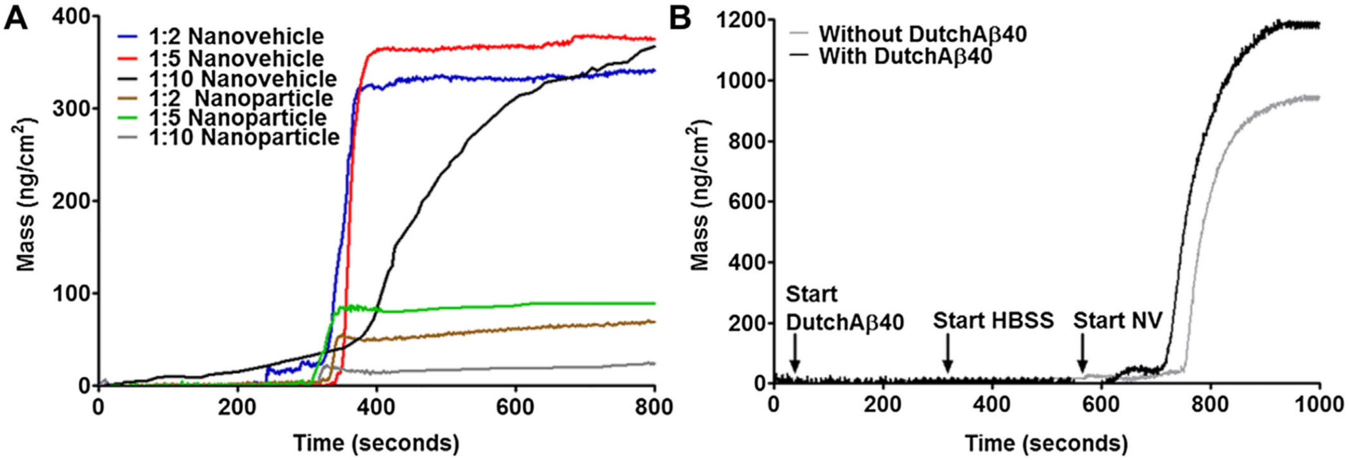

Fig. 3.

(A) Mass change due to adsorption from various dilutions of nanoparticles (without IgG4.1) and nanovehicles (with IgG4.1) to bare gold sensors. **(B)** Mass change due to the uptake of nanovehicles by DutchAβ40-treated (treatment) or HBSS treated (control) Madin Darby canine kidney (MDCK) cells.

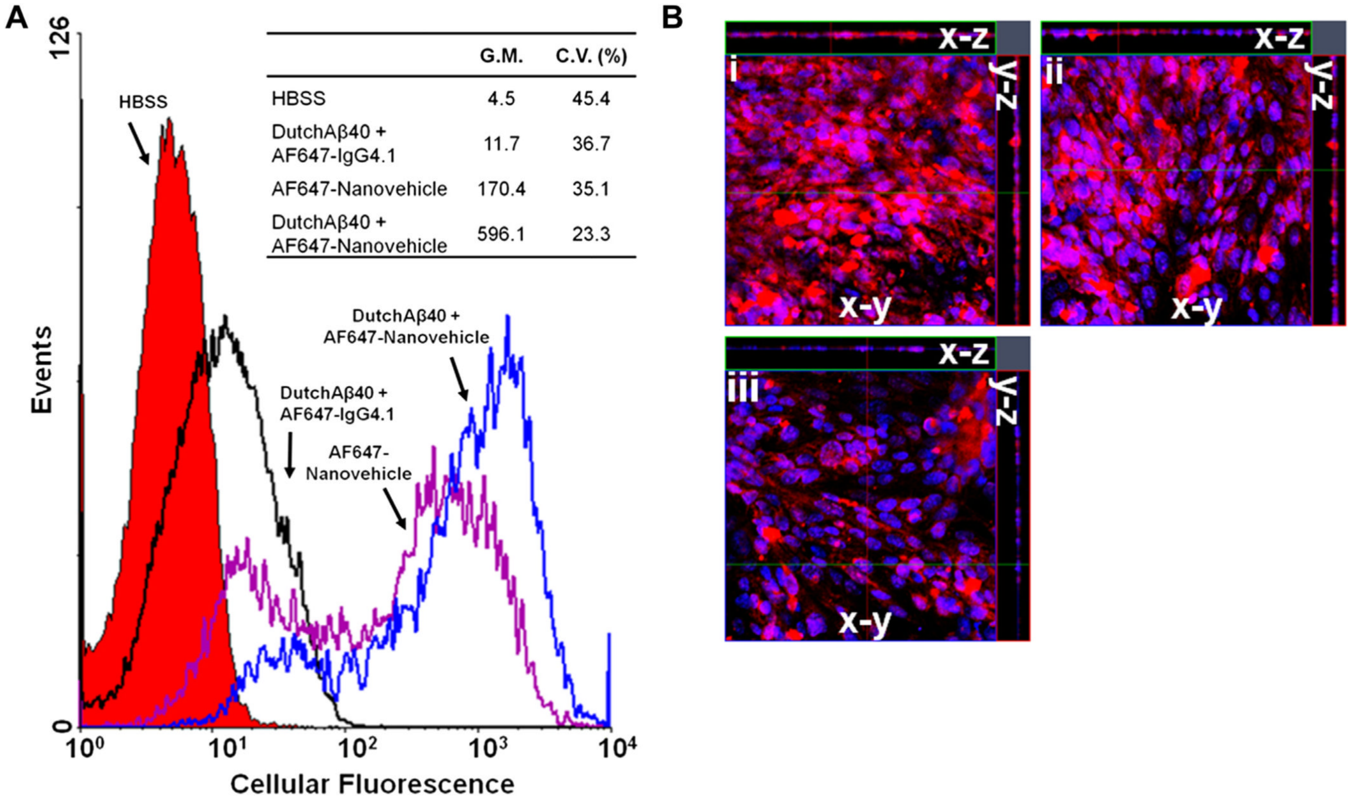

	G.M.	C.V. (%)
HBSS	4.5	45.4
DutchAβ40 + AF647-IgG4.1	11.7	36.7
AF647-Nanovehicle	170.4	35.1
DutchAβ40 + AF647-Nanovehicle	596.1	23.3

Fig. 4.

(A) The uptake of *a)* HBSS- (control), *b)* AlexaFluor647 (AF647)-IgG4.1-, *c)* AF647-nanovehicles in HBSS-, *d)* AF647-nanovehicles in DutchAβ40-treated hCME cells as seen using flow cytometry. G.M. denotes geometric mean and C.V. denotes coefficient of variance. $p < 0.001$: AF647-nanovehicles in DutchAβ40-treated cells as compared to all other treatments. (B) The uptake of i) AF647-nanovehicles in HBSS-, ii) nanovehicles in chlorpromazine- iii) nanovehicles in nystatin- treated human brain microvascular endothelial cell (hCMEC) monolayer as seen using laser confocal microscopy. The x-y plane images were obtained from the center of the z-stack. The AF647-nanovehicles are shown in red fluorescence and the cell nucleus with blue fluorescence. (For interpretation of the references to color in this figure legend, the reader is referred to the web version of this article.)

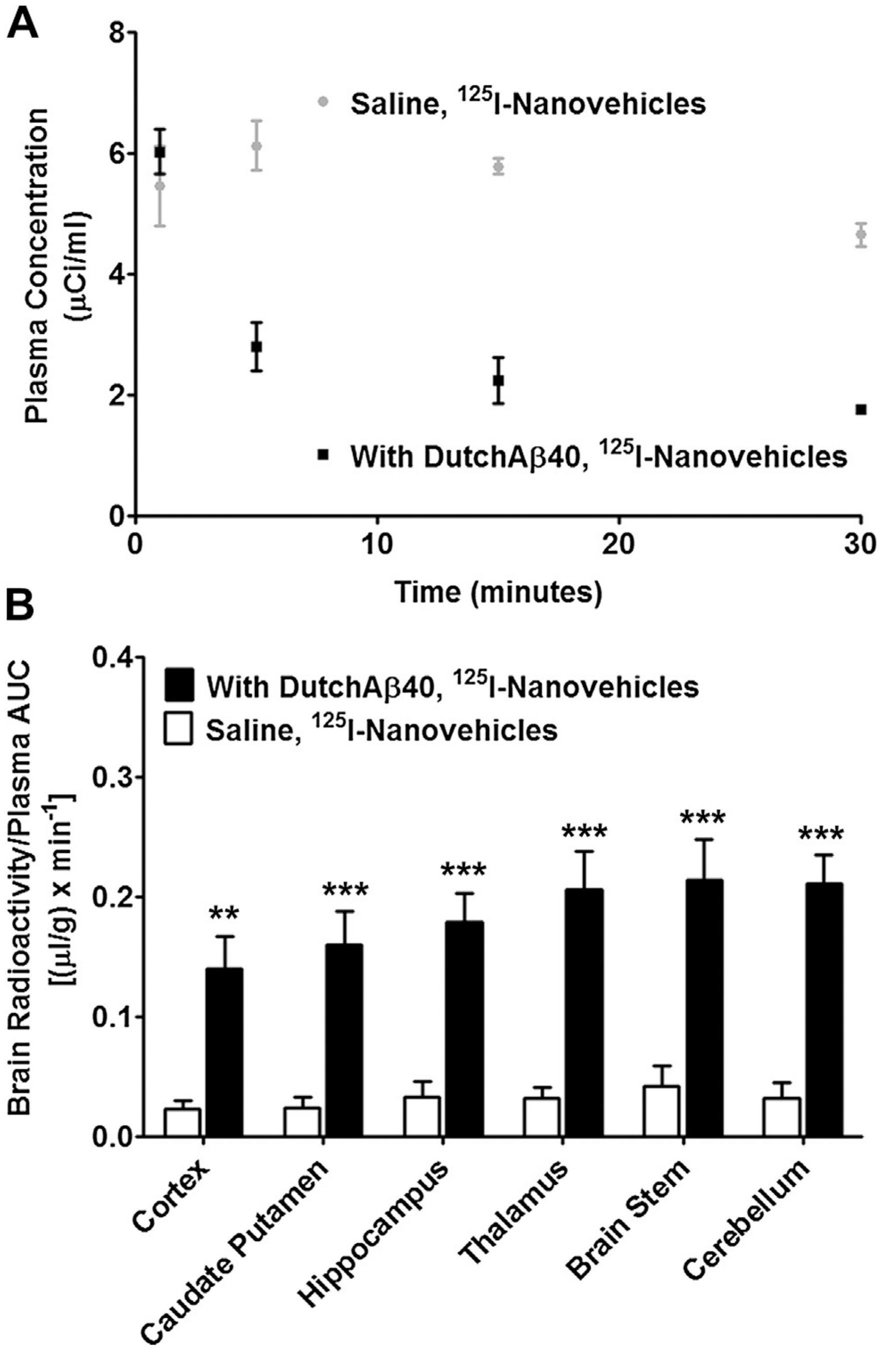

Fig. 5.

(A) The plasma kinetic profile of ^{125}I-nanovehicles in wild type (WT) mice treated with or without DutchAβ40. **(B)** Brain distribution of ^{125}I-nanovehicles in WT mice treated with or without DutchAβ40. $**p < 0.01$ ($n = 3$) or $***p < 0.001$ ($n = 3$); ^{125}I-nanovehicles in DutchAβ40-treated mice vs untreated mice in the respective brain regions.

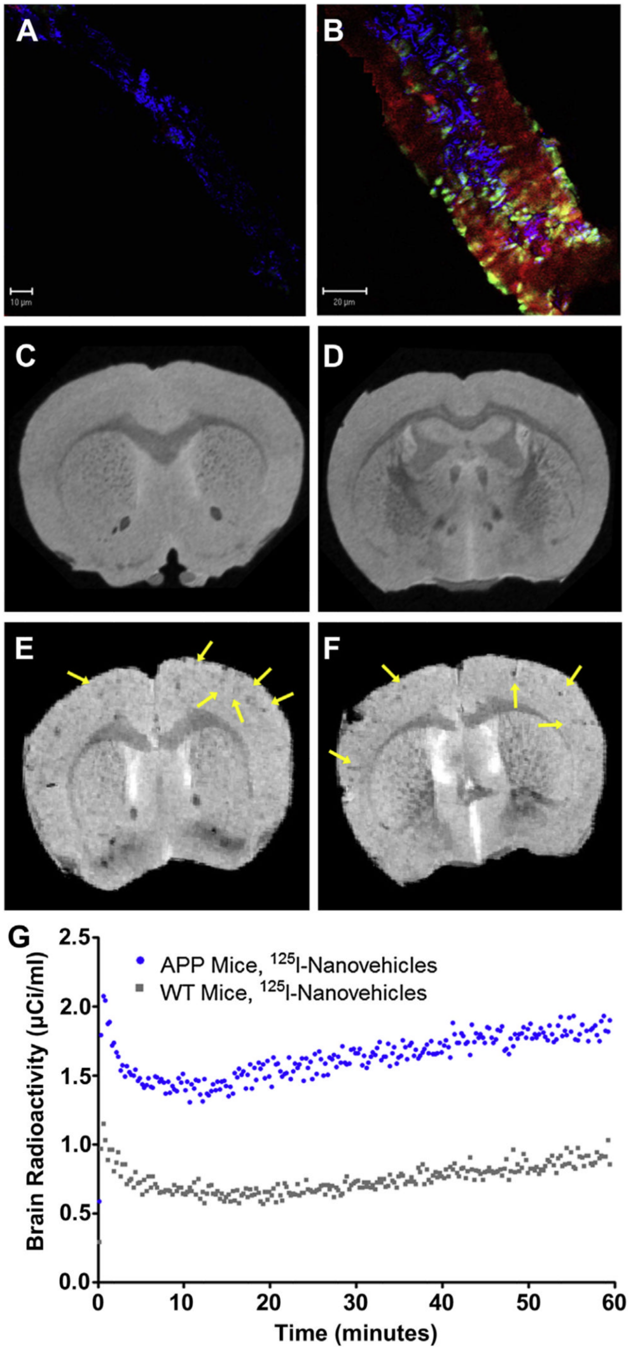

Fig. 6.

Uptake of **(FA)** AlexaFluor 647 (AF647)-nanovehicles in brain arteriole of wild type mouse. **(B)** Uptake AF647-nanovehicles in brain arteriole of APP transgenic mouse. The blue fluorescence is to visualize structure, AF647-nanovehicles emits red fluorescence and Thioflavin S emits green fluorescence. Magnetic resonance imaging of: **(C and D)** Gd-DTPA-nanovehicles in wild type (WT) mice, **(E and F)** Gd-DTPA-nanovehicles in APP transgenic mice. Arrows indicate Gd-DTPA-nanovehicles ability to provide enhanced contrast. **(G)** Brain uptake of ^{125}I-nanovehicles in APP transgenic mice vs ^{125}I-nanovehicles in WT mice as determined by single photon emission computed tomography (SPECT). (For interpretation of the references to color in this figure legend, the reader is referred to the web version of this article.)

Table 1

Plasma pharmacokinetic parameters of ^{125}I-nanovehicles in wild type (WT) mice.

Parameter	**^{125}I-Nanovehicles**		
	With DutchAβ40	**Without DutchAβ40**	***p***
AUC (min × μCi/ml)	309.6 ± 108.3	753.3 ± 129.8	*
Kel (min $^{-1}$)	0.002 ± 0.0009	0.0035 ± 0.0014	N.S.
Cl (ml/min/μCi)	0.077 ± 0.032	0.054 ± 0.012	N.S.
Vdss (ml/μCi)	40.37 ± 5.18	18.79 ± 0.14	**

Data presented as mean ± standard error of the mean.

[*] $p < 0.05$,

[**] $p < 0.01$.

N.S., not significant.

Table 2

Gadolinium (Gd) concentration (mM) and respective T1 and T2 relaxation times.

Nanovehicles (mM Gd)	T_1 (ms)	T_2 (ms)
0.72	2076.7	78.0
1.44	1972.4	77.5
2.87	1694.4	76.4
5.74	1238.7	72.7
11.5	803.8	69.1
23.0	484.1	66.6
Water	2906.3	79.4

Table 3

Relaxivity of nanovehicles at 21.1 T with goodness of fit indicated by adjusted R^2.

	R_1 (mM^{-1}s^{-1})	Adjusted R^2	R_2 (mM^{-1}s^{-1})	Adjusted R^2
NVs	0.072	0.999	1.02	0.91